EDITED BY DOMINIQUE **PENNINCK** AND MARC-ANDRÉ **D'ANJOU**

ATLAS OF SMALL ANIMAL ULTRASONOGRAPHY

THIRD EDITION

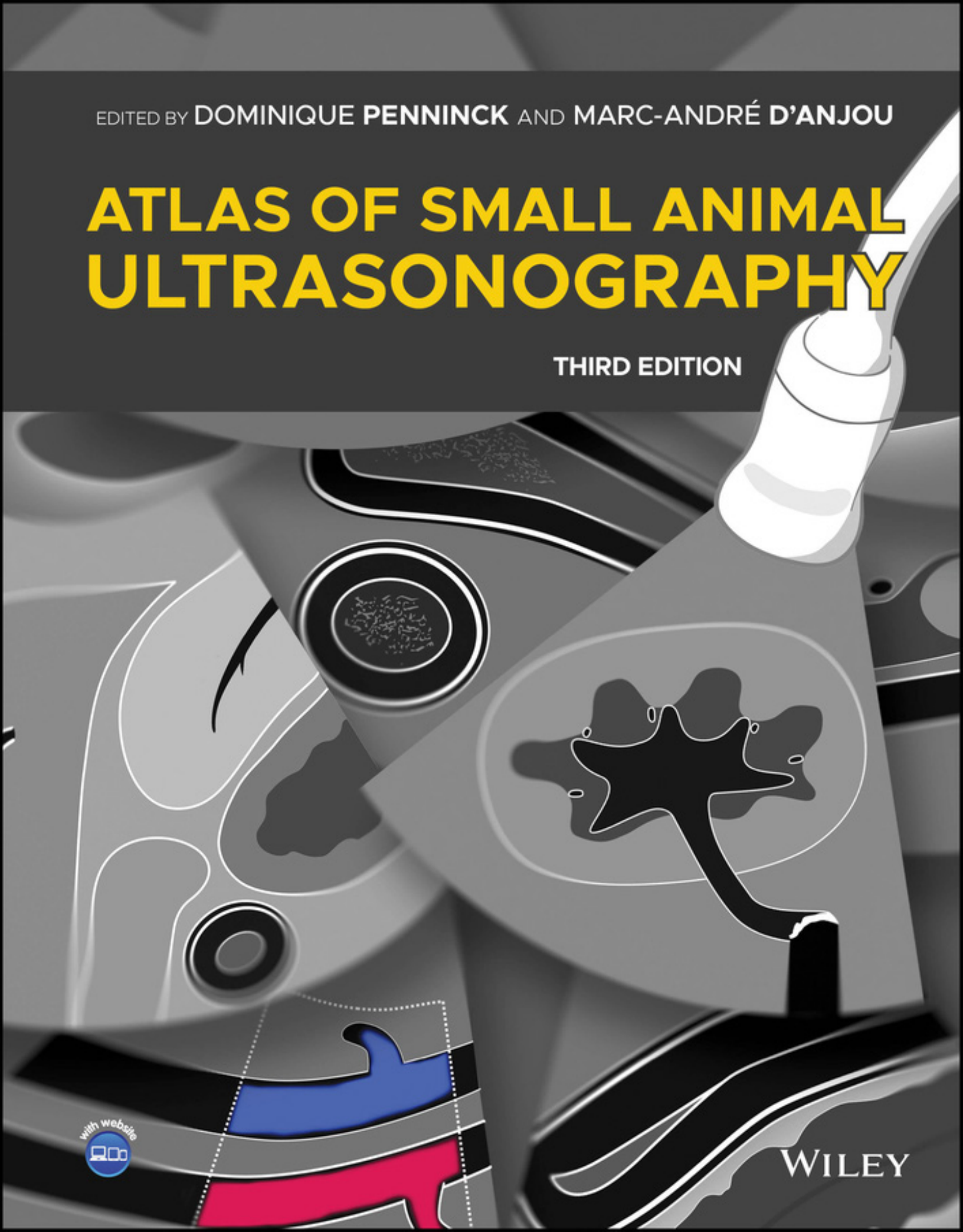

WILEY

Atlas of Small Animal Ultrasonography

Atlas of Small Animal Ultrasonography

THIRD EDITION

Edited by

Dominique Penninck

Department of Clinical Sciences, Cummings School of Veterinary Medicine
Cummings School of Veterinary Medicine, Tufts University
North Grafton, MA
USA

Marc-André d'Anjou

Animages
Brossard, Québec
Canada

WILEY

Published by John Wiley & Sons, Inc., Hoboken, New Jersey.

Published simultaneously in Canada.

The manufacturer's authorized representative according to the EU General Product Safety Regulation is Wiley-VCH GmbH, Boschstr. 12, 69469 Weinheim, Germany, e-mail: Product_Safety@wiley.com.

Library of Congress Cataloging-in-Publication Data applied for

Hardback ISBN: 9781119863267

Cover Design: Wiley
Cover Image: Courtesy of Marc-André d'Anjou

Set in 10/12.5pt Palatino LT Std by Straive, Pondicherry, India

Dedication

To all the pets that kept me sane while glued to the screen during this work.

To my family and friends who stay by my side during difficult times. They rock.

To all the students, residents, and colleagues past, present, and future, for their inspiration.

In memory of my parents, my sisters, and Vincent.

Dominique Penninck

To Annabelle, the roots of my tree.

To Olivier and Héloïse for their inspiring spirit. I am a proud dad.

To all students, interns, residents, and practitioners that show passion for what they do and for whom they want to become.

In memory of Charles and Leo.

Marc-André d'Anjou

Contents

List of Contributors

Mylène Auger
Animages
Brossard, Québec
Canada

Laurent Blond
Centre Hospitalier Vétérinaire Languedocia
Montpellier
France

Søren Boysen
Department of Veterinary Clinical and Diagnostic Sciences
Faculty of Veterinary Medicine
University of Calgary
Calgary, Alberta
Canada

Emmanuelle Butty
Department of Clinical Sciences
Cummings School of Veterinary Medicine
Tufts University
North Grafton, MA
USA

Éric Norman Carmel
Animages
Brossard, Québec
Canada

Marc-André d'Anjou
Animages
Brossard, Québec
Canada

Marilyn Dunn
Interventional Medicine
Faculté de médecine vétérinaire
Université de Montréal
Saint-Hyacinthe, Québec
Canada

Julien Fages
CENTREDMVET
Montréal, Québec
Canada

Hugues Gaillot
ADVETIA Centre Hospitalier Vétérinaire
Vélizy-Villacoublay
France

Mathieu Harel
SONHAR
Veterinary Diagnostic Imaging
Ecully
France

Silke Hecht
Department of Small Animal Clinical Sciences
College of Veterinary Medicine
University of Tennessee
Knoxville, TN
USA

Julie De Lasalle
Animages
Brossard, Québec
Canada

Jonathan Lichtenberger
Pacific Coast Veterinary Cardiology
Victoria, British Columbia
Canada

Wilfried Mai
School of Veterinary Medicine
Section of Radiology
University of Pennsylvania
Philadelphia, PA
USA

Dominique Penninck
Department of Clinical Sciences
Cummings School of Veterinary Medicine
Tufts University
North Grafton, MA
USA

Pascaline Pey
IMPCOM-MEDICAL
Bologna
Italy
and
Antech Imaging Services
Irvine, CA
USA

Stefano Pizzirani
Department of Clinical Sciences
Cummings School of Veterinary Medicine
Tufts University
North Grafton, MA
USA

Shari Raheb
Department of Clinical Studies
Ontario Veterinary College
University of Guelph
Guelph, Ontario
Canada

Delphine Rault
Azurvet Referral Center
Saint Laurent du Var
France

Gabriela Seiler
Department of Molecular Biomedical Sciences
College of Veterinary Medicine
NC State University
Raleigh, NC
USA

Heather Spain
Veritas Veterinary Partners
San Rafael, CA
USA

Swan Specchi
Antech Imaging Services
Fountain Valley, CA
USA
and
AniCura Ospedale Veterinario I Portoni Rossi
Zola Predosa
Italy

James Sutherland-Smith
VetCT
Newton, MA
USA

Chick Weisse
Animal Medical Center
New York City, NY
USA

Preface

Advanced imaging modalities keep evolving and diagnostic ultrasound adapts its place in the clinical diagnostic approach. From initial investigation tool addressing specific clinical questions with a point-of-care approach, to complementary tool assisting interventional procedures, ultrasonography has exponentially grown.

For these reasons, we modified the previous Atlas contents to include a chapter on point-of-care ultrasound, a chapter solely dedicated to abdominal vascular studies and added updated information on ultrasound-guided interventional procedures, where it best applies. This edition has a total of 17 chapters and a companion website complements the textbook with numerous annotated video clips. Beyond these changes, new clinical cases with high-quality images were added to reflect what are commonly and less commonly encountered disorders, along with recently cited literature.

Our group of collaborators grew to embrace the larger community of sonographers.

That said, we warmly acknowledge and thank the contributors of the past editions who participated in setting the foundation of this book. As for the past edition, we solicited your comments and suggestions, and incorporated most of them in this third edition.

Supporting annotated video clips referred to in the Atlas can be found on the website *SmallAnimal Ultrasonography.com*. This resourceful website contains supplementary educative material that complements the Atlas and goes beyond.

Cordially on the same wavelength,

Dominique Penninck and Marc-André d'Anjou

Accompanying Videos

Some concepts are better explained using movies and this is particularly true for ultrasound. We therefore offer a collection of videos for each chapter, each with annotations and some with voice over, covering normal sonographic anatomy and features of common diseases. These video clips can be found in our website www.SmallAnimalUltrasonography.com, under ***The Book/Atlas videos*** section, using the password: **gbh3972pxe**.

To expand your knowledge on common and less common diseases, you can subscribe to a larger collection of videos (260+) under ***Video Memberships*** (sign-up details online).

Chapter 1 – Practical physical concepts and artifacts

- Image formation and other principles
- Propagation of US waves and interaction with tissues
- US beam and spatial resolution
- Gain, TGC and other manual adjustments
- Mirror image artifact
- Shadowing artifact
- Enhancement artifact
- Reverberation artifact
- Refraction artifact
- Speed error and range ambiguity artifacts
- Twinkle artifact

Chapter 2 – Point of care US

- Lung sliding
- B-lines that occur secondary to increased lung density
- Lung point
- Abnormal curtain signs
- Air and fluid bronchograms
- Subxiphoid view of the heart and active cardiac compressions during cardiopulmonary resuscitation in a cat.

Chapter 3 – Eye and orbit

- Normal eye anatomy and scanning
- Asteroid hyalosis
- Cataracts
- Retinal detachment
- Lens luxation
- Lens extrusion
- Intra-ocular neoplasia
- Retrobulbar foreign body

Chapter 4 – Neck

- Normal neck anatomy and scanning
- Thyroid carcinoma
- Parathyroid nodule
- Lymphadenopathy
- Neck abscess and foreign body
- Neck abscess
- Salivary sialocele

Chapter 5 – Thorax

- Normal lung interface
- Thoracic wall mass
- Pleural effusion
- Pulmonary mass
- Mediastinal mass
- Branchial cyst
- Diaphragmatic hernia

Chapter 6 – Heart

- Normal short and long axes of the heart (dog)
- Normal short and long axes of the heart (cat)
- Chronic degenerative valvular disease
- Hypertrophic cardiomyopathy in a cat
- Dilated cardiomyopathy in a dog
- Pulmonary hypertension/cor pulmonale in a dog
- Idiopathic pericardial effusion and tamponade in a dog

- Cardiac tumor
- Patent ductus arteriosus in a dog
- Pulmonic stenosis in a dog
- Subaortic stenosis in a dog
- Ventricular septal defect in a cat

Chapter 7 – Hepatobiliary

- Normal liver and biliary system
- Lipidosis
- Steroid-induced and other vacuolar hepatopathies
- Nodular hyperplasia
- Chronic active hepatitis
- Cholangitis /cholangiohepatitis in cats
- Cirrhosis
- Hepatocellular carcinoma
- Hepatic metastases
- Hepatic lymphoma
- Cystadenoma
- Gallbladder mucocele
- Extrahepatic biliary obstruction
- Gallbladder sludge
- Cholelithiasis

Chapter 8 – Spleen

- Normal spleen anatomy and scanning
- Myelolipomas
- Splenic lymphoma
- Nodular hyperplasia and extramedullary hematopoiesis
- Hemangiosarcoma and peritoneal effusion
- Splenic torsion
- Splenic venous thrombus and infarcts

Chapter 9 – Gastrointestinal tract

- Normal GI anatomy and scanning
- Intussusception
- Foreign bodies
- Enteritis
- Lymphangiectasia
- Ulceration
- Lymphoma
- Carcinoma
- Mesenchymal tumor

Chapter 10 – Pancreas

- Normal pancreas
- Pancreatitis in dogs
- Pancreatitis in cats
- Pseudocyst
- Necrotizing pancreatitis in dogs
- Pancreatic carcinoma
- Insulinoma

Chapter 11 – Urinary tract

- Normal kidneys
- Chronic interstitial nephritis
- Acute nephritis
- Pyelonephritis
- Renal lymphoma
- Renal primary neoplasia
- Polycystic renal disease
- Perinephric pseudocyst
- Obstructive nephrolithiasis and hydronephrosis
- Ectopic ureters
- Normal bladder and urethra
- Cystitis
- Polypoid cystitis
- Calculi
- Blood clot
- Ureteral jet
- Bladder tumors

Chapter 12 – Adrenal glands

- Normal adrenal glands in a dog
- Normal adrenal glands in a cat
- Adrenal hyperplasia with PDH in dogs
- Adrenal adenoma and adenocarcinoma in dogs
- Adrenal pheochromocytoma in a dog

Chapter 13 – Repro female

- Normal ovaries and uterus
- Normal pregnancy: different stages
- Pyometra
- Cystic endometrial hyperplasia

Chapter 14 – Repro male

- Scanning of the normal male reproductive tract in a dog
- Benign Prostatic Hyperplasia
- Prostatic tumor
- Prostatic abscess
- Testicular tumor

Chapter 15 – Abdominal cavity and lymph nodes

- Normal abdominal wall, cavity, fat and lymph nodes
- Peritoneal effusions
- Mesenteric mass
- Peritonitis
- Carcinomatosis
- Lymphadenopathy
- Abdominal wall and umbilical hernia

Chapter 16 – Abdominal vasculature

- Normal portal system
- Normal abdominal major vasculature
- Portosystemic shunts
- Vascular thrombosis

Chapter 17 – Musculoskeletal system

- Normal shoulder: Scanning technique & Anatomy (dog)
- Normal common calcaneal tendon
- Bicipital tenosynovitis
- Supraspinatus tendinopathy
- Common calcaneal tendinopathy
- Gracilis myopathy in a dog
- Osteomyelitis
- Joint neoplasia
- Supraspinatous/infraspinatous abscess in a dog
- Peripheral nerve sheath tumor
- Vertebral mass invading the spinal canal

CHAPTER ONE

Practical Physical Concepts and Artifacts

Marc-André d'Anjou[1] and Dominique Penninck[2]

[1]*Animages, Brossard, Québec, Canada*
[2]*Department of Clinical Sciences, Cummings School of Veterinary Medicine, Tufts University, North Grafton, MA, USA*

Fundamentals

Sound is a series of vibrations transmitted through an elastic solid, a liquid, or a gas. Sound waves have variable wavelengths and amplitudes, with a frequency defined as being the number of cycles repeated over a given time interval. A high frequency sound therefore has a shorter wavelength and more cycles per second than a low frequency sound. The human ear can perceive sounds in the range of 20–20,000 cycles per second or up to 20 kHz. Beyond this range, it is called "ultrasound." Ultrasound frequencies used in medical imaging generally vary between 3 and 12 MHz, or 3–12 million cycles per second, which is well beyond what the human ear can perceive.

Electronic linear probes are equipped with a row of **piezoelectric crystals** whose alignment varies from flat (or linear) to convex. The material contained in each one is deformed when it receives an electrical charge and emits a vibration: this is the initial ultrasound pulsation. The ultrasound wave travels through the tissues, generating several returning waves or echoes that upon reaching the probe make the crystals vibrate again, producing a new electric current that travels to the system's computer and provides information on the type of each of the deflected waves. The set of all the deflected waves creates the ultrasound image.

To produce an **image**, the first piezoelectric crystals are stimulated to generate a short ultrasound pulse – consisting of three to four waves – at a precise angle, producing thousands of echoes that are sent back to the probe (Figure 1.1). Shortly after, a new ultrasound pulse leaves the probe at a different angle, generating a new set of echoes that return to the second series of crystals. Assuming a constant wave propagation speed of 1540 m/s in soft tissues, each of these echoes can be located precisely along the trajectory, depending on the time interval between the departing wave and the returning wave. Hundreds of wave lines are produced this way, scanning tissues at high speed to produce over 30 images per second, each one containing thousands of pixels describing the acoustic characteristics of the scanned tissues.

Tissue acoustic characteristics are defined by the **acoustic impedance**, which dictates their level of ultrasound reflection and thus their echogenicity. Impedance is the product of the speed of ultrasound waves through a given tissue multiplied by its density (Table 1.1) (Bushberg et al. 2011). Ultrasound wave reflection is stronger at interfaces of tissues with opposed acoustic impedance, and weaker when traversing an interface of tissues with similar acoustic impedances. Mild variations in acoustic impedance are desirable for tissue examination, resulting in variable echogenicity and echotexture that allow internal architectures to be compared. In fact, not only does the ultrasound system locate the origin of each echo, it also measures its intensity, which is expressed in terms of pixel brightness on the unit monitor (B mode).

Normal **tissue echogenicity** that varies among organs and structures (Figure 1.2) and damaged tissue with altered acoustic characteristics, can be compared. Normal and abnormal structures can be defined in terms of echogenicity as hypoechoic or hyperechoic to their normal state, or to other structures to which they are compared. Fluids without cells or large particles

Atlas of Small Animal Ultrasonography, Third Edition. Edited by Dominique Penninck and Marc-André d'Anjou.

Companion website: www.SmallAnimalUltrasonography.com

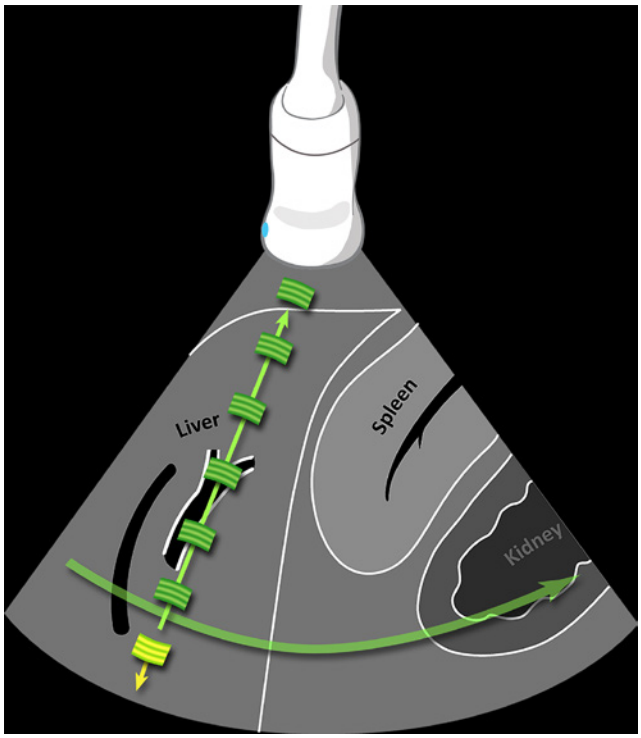

Figure 1.1. Ultrasound propagation and image formation. Each ultrasound image is formed by the addition of hundreds of individual scan lines. Each line is produced after a single ultrasound pulse (in yellow) is emitted by the transducer. As this pulse propagates through soft tissues, many echoes (in green) are generated at interfaces of different acoustic impedance (such as *hepatocytes-connective tissue*), producing an image of variable echogenicity and echotexture. Each echo is anatomically localized based on the time interval between the emitted pulse and its reception. After a specific time, a new pulse is emitted along an adjacent line, producing an additional scan line. Scan lines are generated very rapidly and successively, producing 15–60 images per second, allowing "real-time" ultrasonography.

Table 1.1
Density and speed of sound in materials and biological tissues and resulting acoustic impedance

Material or tissue	Density (kg/m^3)	Speed (m/sec)	Acoustic impedance
Air	1.2	330	0.0004×10^6
Lung	300	600	0.18×10^6
Fat	924	1,450	1.34×10^6
Water	1,000	1,480	1.48×10^6
Soft tissues (in general)	1,050	1,540	1.62×10^6
Liver	1,061	1,555	1.65×10^6
Kidney	1,041	1,565	1.63×10^6
Skull bone	1, 912	4,080	7.8×10^6

Source: Bushberg et al. (2011).

are anechoic, i.e., totally black, because of the absence of reflectors.

Interactions between ultrasound waves and tissues and materials vary, dictating the intensity of echoes generated and the residual intensity of the pulse that pursues its course through tissues (Hangiandreou 2003) (Figure 1.3). For instance, ultrasound waves penetrating fat result in ***acoustic diffusion*** as the primary interaction, reducing the intensity of the initial pulse. This type of interaction also explains the echotexture – i.e., granularity – of the parenchyma that varies among organs. On the other hand, the interaction with a smooth interface that is perpendicular to the beam axis, such as the renal capsule in Figure 1.3, causes ***specular reflection***, which produces intense echoes in the opposite direction of the initial pulse. Some materials like mineral absorb a significant component of the initial pulse energy that becomes too weak to generate echoes from deeper tissues. Ultrasound ***absorption*** can then cause a shadow (see *Artifacts*). Finally, ultrasound waves may change in direction due to ***refraction***. In reality, these types of interactions are often combined, and their presence and relative importance is mainly influenced by the differences in acoustic impedance and by the shape of the tissue (or material) interfaces. These interactions cause the emitted ultrasound pulse energy to eventually become completely dissipated.

Ultrasound Probes and Resolution

Ultrasound probes vary in configurations for specific needs (Figure 1.4). Curved linear probes, also called convex or microconvex, have one or several rows of piezoelectric crystals aligned along a convex surface, with varying beams and paths. These probes produce a triangular image because of the diverging lines of ultrasound waves they generate. The main assets of this type of probe are its smaller curve and its large scanning coverage, making it the ideal probe for assessing

the abdomen, particularly the cranial portion along the rig cage. The piezoelectric crystals of the linear probes are distributed along a flat surface, producing a rectangular scan field. The phase interval of the impulsions can also produce a trapezoid-shaped image, allowing it to cover a larger surface. This is especially useful when evaluating superficial organs whose dimension may be greater than the width of the scanned area, such as the kidneys and spleen. The length of the probe's track indicates the width of the area it scans.

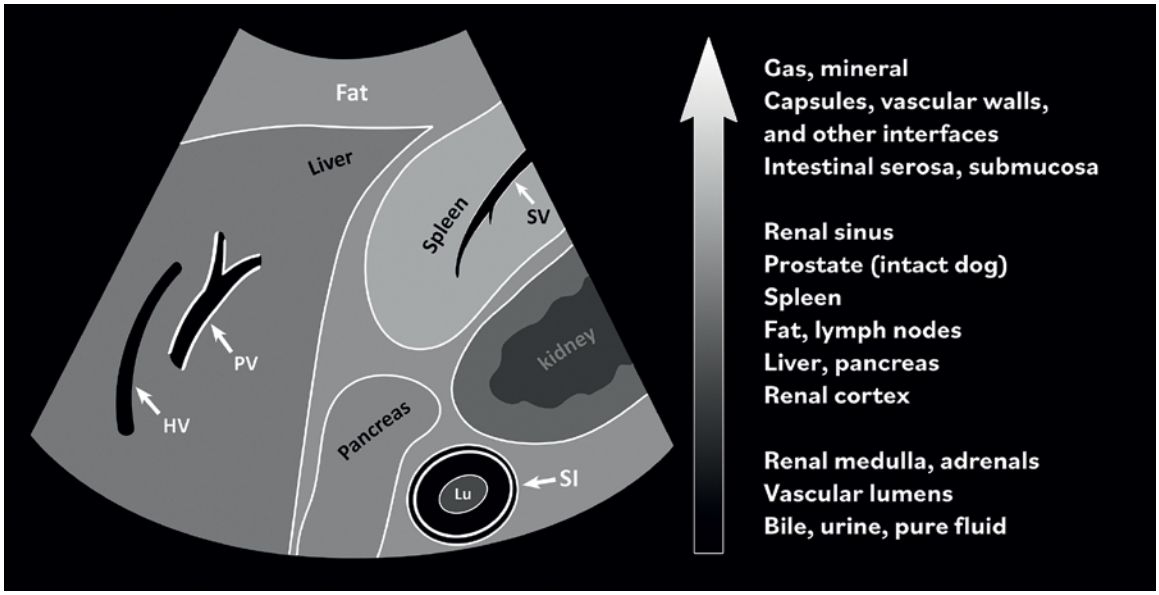

Figure 1.2. **Relative echogenicity of tissues and other materials.** Structures can be recognized and differentiated by their echogenicity. This figure illustrates the relative echogenicity of normal abdominal structures in dogs and cats. Note that the walls of the portal vein (PV) are hyperechoic even when this vein is not perpendicular to the insonation beam, differing from the adjacent hepatic vein (HV). The splenic vein (SV) walls become hyperechoic when perpendicular to the beam. The fluid in the small intestinal (SI) lumen (Lu) is not fully anechoic because of the ingested particles. The renal cortex is often hyperechoic in normal dogs and cats and may become isoechoic to the liver and even to the spleen. The adrenal medulla may be hyperechoic in certain normal animals, sometimes exceeding the echogenicity of the renal cortex. It is important to point out that tissue echogenicity may also be influenced by several equipment-related factors, such as transducer frequency and orientation, focal zone number and position, etc.

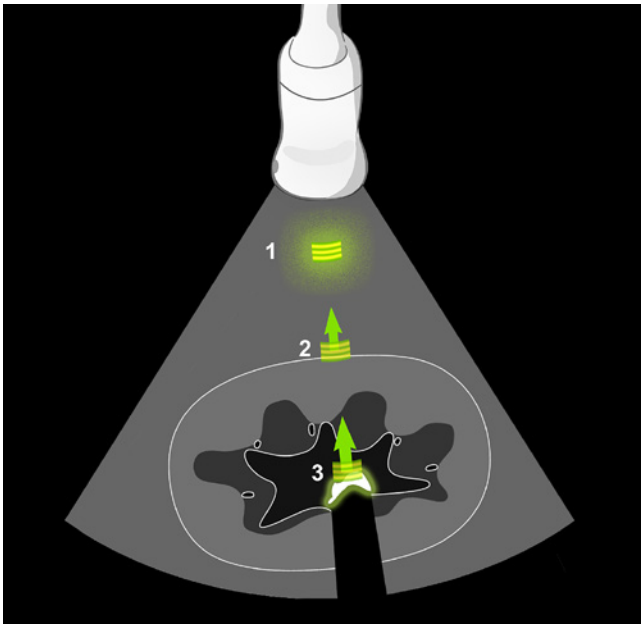

Figure 1.3. **Interactions between ultrasound waves and tissues.** The emitted ultrasound pulse is charged with energy. In this example, the pulse initially interacts with the abdominal fat (1) causing acoustic diffusion and partly losing its energy as it continues its course. When interacting with a smooth, linear interface such as the renal capsule (2), a strong specular reflection occurs that generates a highly intense echo (green arrow). The weaker ultrasound pulse (3) then reaches the renal pelvic calculus that absorbs most of the wave energy, while causing a strong reflection (green arrow). An acoustic shadow is generated, and the initial pulse energy is completely dissipated.

Figure 1.4. Practical ultrasound transducers. Most ultrasound units are equipped with convex (A, B) and linear (C) electronic transducers with variable frequencies. A macroconvex probe offering lower frequencies (3–8 MHz) is best suited for the abdomen of large dogs, whereas a microconvex probe (B) of higher frequency and smaller footprint is preferred for the abdomen of small patients and when only a small acoustic window is available (e.g., intercostal approach of a lung lesion). A high-frequency (10–18 MHz) linear probe is most useful for assessing superficial structures on a relatively wide and flat surface (e.g., assessing bowels in a cat, biceps tendon in a dog). A phased array transducer (D) offers a small flat footprint and is ideal for echocardiography.

Spatial resolution is the ability of a system to recognize and distinguish between two small structures located close together. For instance, optimal spatial resolution allows us to distinguish between two small nodules in the liver instead of mistaking them for only one or missing a lesion that is adjacent to a normal structure. The spatial resolution along the path of the ultrasound beam – the *x* axis – is determined by the length of the pulse, which in turns is related to wave frequency (Figure 1.5). As the ultrasound frequency remains constant in depth, so does the axial resolution. Conversely, lateral (*y* axis) and slice-thickness (*z* axis) resolutions vary in depth as the ultrasound beam changes in shape to narrow at the level of the focal zone (Figure 1.6). For a given probe, the axial resolution is generally superior to lateral or slice-thickness resolutions, justifying those measurements be obtained whenever possible along that *x* axis.

Contrast resolution is the same system's ability to differentiate structures that present small differences in acoustic behavior (Figure 1.7). The influence of these two types of resolution is significant and hinges on image quality, the ability to evaluate structures and to detect and describe lesions.

As seen before, ultrasound waves interact with tissues in different ways causing the initial pulse to progressively lose its intensity in depth. This attenuation limits contrast resolution in deeper areas, particularly

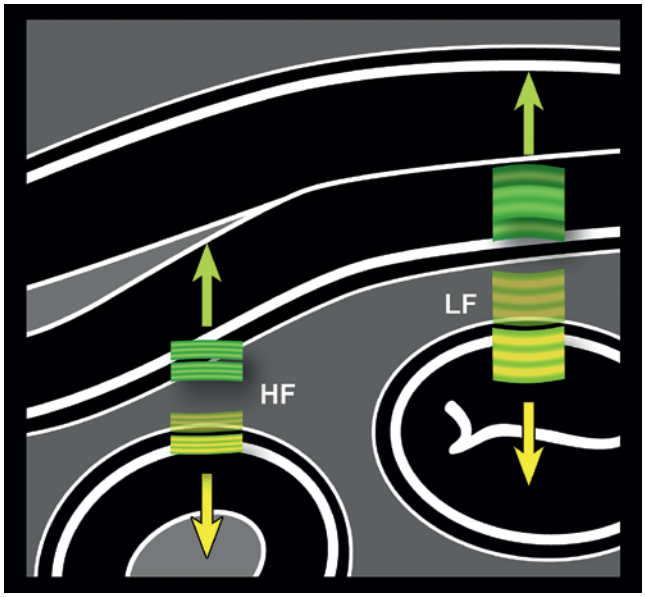

Figure 1.5. Ultrasound frequency versus axial resolution. The higher the frequency, the shorter the pulse. Because the length of the pulse does not change in depth or after interaction with tissues, high-frequency (HF) echoes that come back to the transducer are better discriminated by the system. Closely associated interfaces, such as small intestinal wall layers are then better represented. Conversely, echoes from closely aligned layers generated by a low-frequency (LF) pulse partly overlap and are interpreted by the system as originating from a single interface. This phenomenon is exaggerated in this illustration for better comprehension of this important concept.

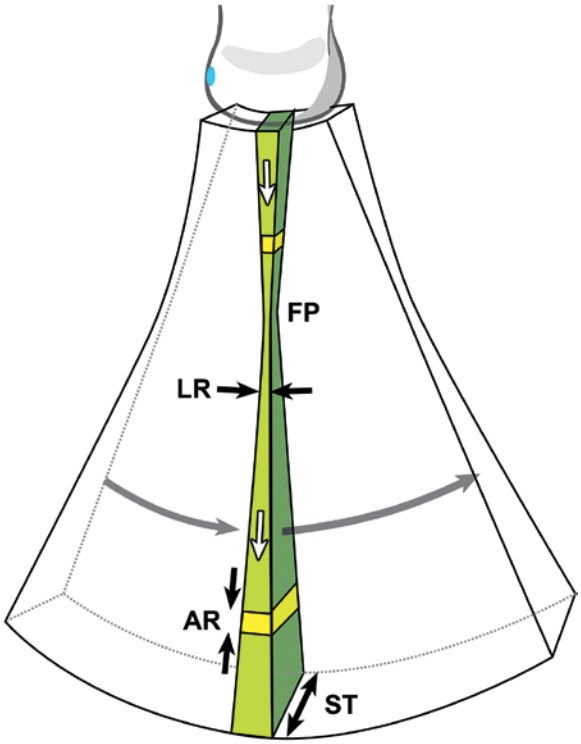

Figure 1.6. Shape of the ultrasound beam in depth. The ultrasound beam is larger at its emission point (piezoelectric elements) before narrowing at the focal point (FP), and becoming larger again further in depth. This change in shape affects the lateral resolution (LR, i.e., beam width) and slice-thickness (ST, elevational resolution), but does not affect the axial resolution (AR), which is dictated by the pulse frequency that remains constant in depth. Generally, the axial resolution is superior to the other resolutions.

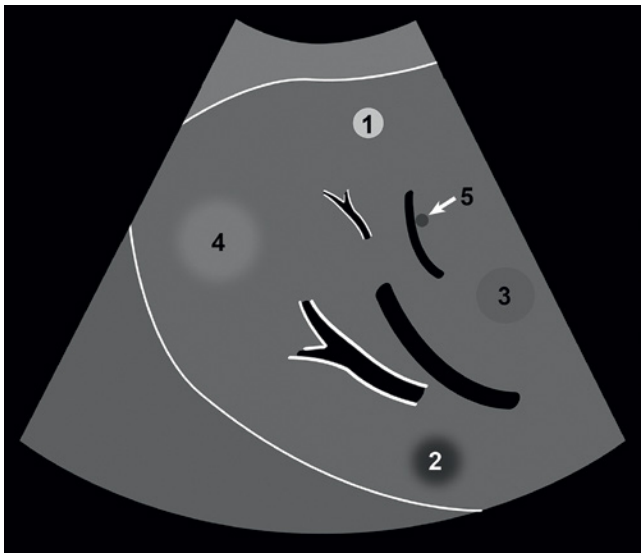

Figure 1.7. Spatial and contrast resolutions. The capacity of an ultrasound system to detect and distinguish structures of small size and similar acoustic characteristics greatly influenced its diagnostic capability. In this illustration, the hyperchoic nodule 1 is clearly depicted. Its characteristics (size, echogenicity, and margin) favor its identification. The hypoechoic nodule 2 is also visualized due to its size and marked hypoechogenicity but has ill-defined contours. Nodules 3 and 4 are larger but less conspicuous because of their echogenicity that is similar to the regional liver parenchyma. Contrast resolution of the system – and certain image adjustments – dictates its capacity to identify structures of characteristics that are similar to the background. The small hypoechoic nodule 5 is differentiated from the adjacent hepatic vein because of sufficient spatial resolution. Lower spatial resolution would cause this nodule to be confused with the vessel.

when using high frequency probes. Indeed, the coefficient of attenuation of ultrasound waves through tissues increases in direct proportion to wave frequency. This can be particularly problematic in certain animals, such as large obese dogs, or with certain disease processes (e.g., lipidosis). The use of lower frequency probes can partially compensate for this loss of signal, but to the cost of reduced detail (lower spatial resolution). Generally, the probe offering the highest frequency but allowing all desired tissues to be imaged with sufficient signal should be selected.

System Adjustments and Image Quality

Images can be frozen to take measurements and add text, prior to recording still or looped images that can be archived or submitted to a colleague for another opinion. But prior to be recorded, images must be optimized. Except for automatic processes, many adjustments can and should be made manually throughout the examination. Changes in tissue depth and acoustic properties require constant adjustments.

The **gain** determines the level of amplification of echoes to compensate for their attenuation in tissues, increasing the brightness of corresponding pixels on the screen. It can be adjusted generally or modulated specifically in depth (Figure 1.8). Time-gain compensation (TGC) is adjusted through sliding knobs, reducing superficial amplification, or increasing depth amplification, for instance. Since ultrasound attenuation will vary from one animal to another and from one abdominal region to another depending on the acoustic characteristics of normal and abnormal tissues, both the general gain and TGC will have to be adjusted during the examination. Recent ultrasound units offer automatic gain adjustment that can serve as a start for further micro adjustment.

Image field **depth** determines the length of the long axis, allowing the same structure to be imaged

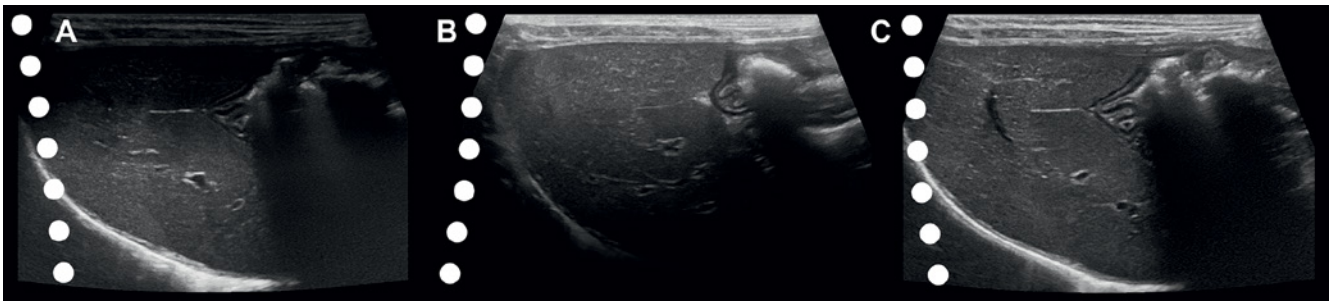

Figure 1.8. **Gain setting.** Because of the attenuation of the ultrasound beam as it travels through soft tissues, the amplification of echoes received must be adjusted according to tissue type and depth. This modulation can be made using time-gain compensation cursors. These three images show the variation in echogenicity of a normal liver with **(A)** insufficient near gain and excessive far gain, **(B)** excessive near gain and insufficient far gain, and **(C)** well-adjusted near and far gains. The lines of dots correspond to the time gain-compensation cursors that were adjusted to obtain each ultrasound image.

completely, or partly. This also needs to be adjusted continually to maximize the visualization of structures in the region of interest.

The ultrasound beam can be electronically **focalized** to reduce its diameter at a specific depth. In the focal zone, the beam's width and thickness are considerably reduced, increasing the capacity of the system to depict small structures along the y (lateral) and *z* (slice-thickness) planes, respectively (see Figure 1.6). Moreover, the intensity of the beam is concentrated over a small area, increasing the signal from tissues in that region, favoring contrast resolution. On recent systems, the focal zone is automatically adjusted during the exam, but, if possible, the focal zone should be manually adjusted during examination at the depth of the region of interest. By using two (or more) focal zones, the beam is narrowed over a greater distance, increasing the spatial and contrast and contrast resolution over a longer depth. The downside however is that using more zones requires more time, thereby reducing frame rate which may limit the examination of moving structure. Multifocal optimization is easier while evaluating structures that are completely immobile.

Noise is an inherent part of all imaging procedures and can become problematic in large patients or when using low-end systems. It results from insufficient signal (i.e., echoes) emanating from tissues and reaching the ultrasound probe, from electric interferences, from artifacts (see *Artifacts*), or from improper signal processing by the unit. The result is a coarse-grained textured and/or greyish image that does not represent normal tissue anatomy, and which limits our ability to view shades of grey (reduced contrast resolution). Noise can be partly reduced by using a higher frequency probe, by switching to the harmonic or compound imaging modes, or by increasing output power.

Spatial compound imaging (which vary in name among brands) refers to the electronic steering of ultrasound beams from an array transducer to image the same tissue multiple times by using parallel beams oriented along different directions (Figure 1.9). Tissues are scanned from different angles, simultaneously, allowing multiple echoes from the same tissue interfaces to be collected and combined, increasing the overall signal and reducing noise. Image contrast is increased, and tissue interfaces become more conspicuous. Tissues boundaries are better outlined and since background noise is reduced, cystic lesions, for instance, are fully anechoic ant thus more easily differentiated from solid lesions. On the other hand, certain useful artifacts such as acoustic shadowing – which helps recognizing mineral for instance – may be less apparent when compound imaging is used. Because multiple ultrasound beams are used to interrogate the same tissue region, more time is required for data collection, reducing the frame rate when compared with that of conventional B-mode imaging. This mode may limit the examination of moving patients.

The **harmonic mode** also increases tissue contrast by selecting echoes at a specific frequency. The term harmonic refers to frequencies that are integral multiples of the frequency of the transmitted pulse (which is also called the fundamental frequency, *f*, or first harmonic). Harmonic frequency echoes ($1/2f$, $2f$, etc.) develop because of the distortion of the transmitted pulse as it travels through tissues (Ziegler and O'Brien 2002). The initial pulse in fact deforms from a perfect sinusoid to a sharper, sawtooth shape, generating reflected echoes of several different frequencies. The use of higher-order harmonic echoes instead of

the fundamental echoes results in improved image contrast and reduced noise, increasing normal and abnormal tissue conspicuity. The reduction of artifacts and clutter is most efficient in the near field (Figure 1.10). This may prove particularly valuable in large patients with thick abdominal walls and subcutaneous fat planes.

Finally, several other aspects can influence the quality of ultrasound images. As for digital radiographs, the quality of the unit monitor (size, dynamic range, brightness, calibration) can influence our ability to accurately assess ultrasound images. Several features can be used and modulated to create scanning presets, for different types of patients or body parts. Sonographers must be aware of the strengths and limitations of their system.

The **extended field of view** (also called **panoramic mode**) imaging allows to obtain panoramic images of several structures/organs or masses that would otherwise not fit in one conventional field of view (Figure 1.11). Measurements can then be performed and were shown to be reliable (Liu et al. 2022). Clinical applications described in humans mostly evolve around the musculoskeletal system (Fitze et al. 2023), obstetric and breast, but it can be applied to any body parts.

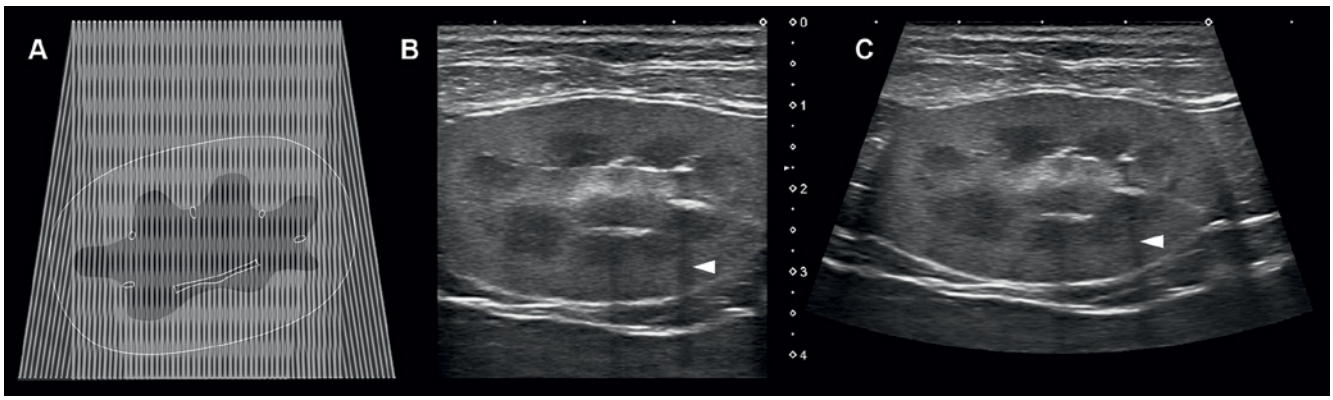

Figure 1.9. **Spatial compound imaging. (A)** With this mode, the same tissue is scanned using different beam angulations (steering) to produce a trapezoidal image that is wider than the footprint of the transducer. **(B, C)** Superficial structures such as this kidney may exceed the size of the image field when the standard linear mode **(B)** is used, whereas spatial compounding expands the width of the image to include the kidney that can be fully assessed and measured **(C)**. Beam angulation also influences the shape of shadowing artifacts (arrowheads).

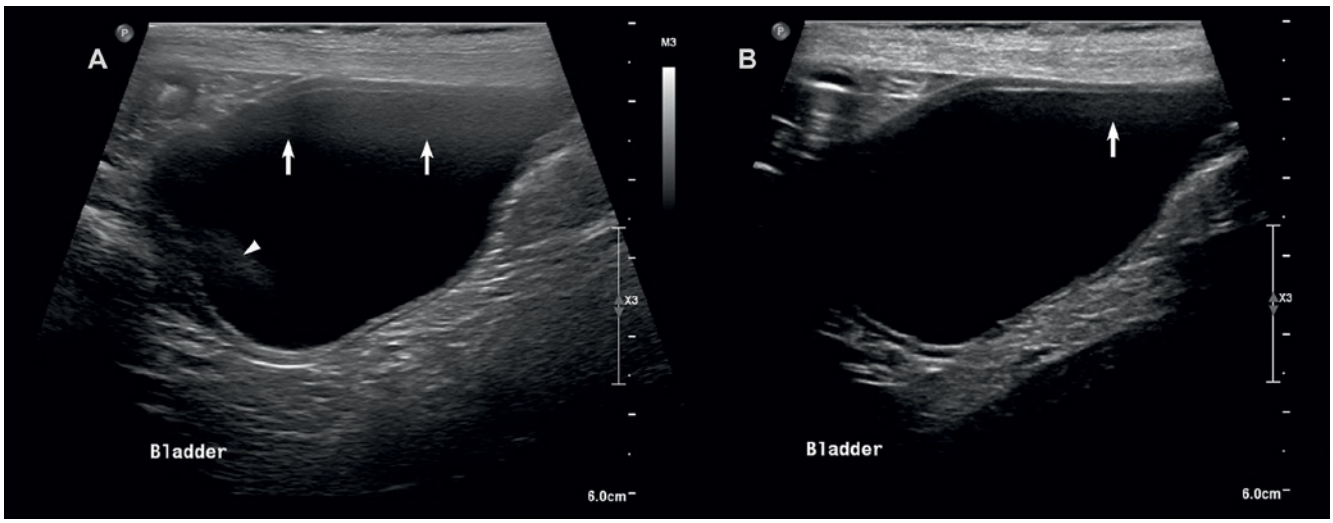

Figure 1.10. **Harmonics mode. (A)** Without this mode, the near field of the image of a bladder is blurred with faintly echogenic artifacts (arrows). Side-lobe artifacts are also more apparent (arrowhead) **(B)** With Harmonics mode, the near field appears crisp, and the outline of the bladder is clear. Near-field artifacts are greatly reduced, and side-lobe artifacts are no longer visible.

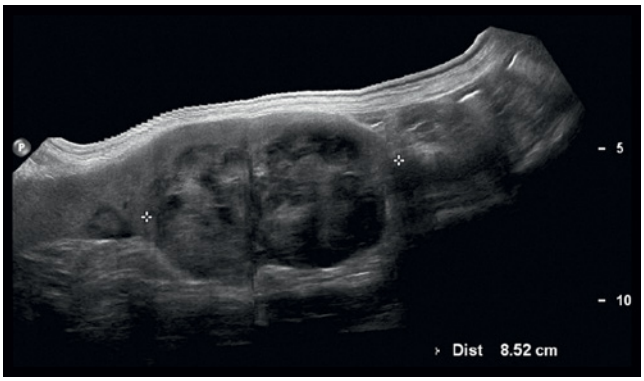

Figure 1.11. Panoramic mode (extended view). 8.5 cm long inhomogeneous abdominal mass is confirmed to originate from the spleen of this dog. The panoramic mode facilitates the measurements of any large mass that exceed the standard field of view. Notice the long and serrated contact line that is the result of manual displacement of the probe.

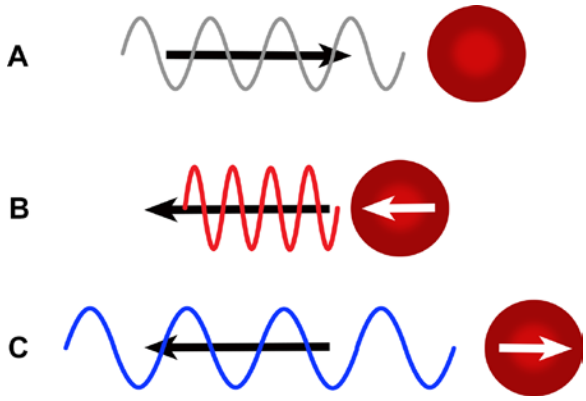

Figure 1.12. Doppler effect. (A) The ultrasound pulse emitted by the probe moves in direction of a red blood cell (RBC) at a specific frequency. **(B)** If the RBC moves toward this pulse, a positive Doppler shift occurs, increasing the frequency of the returning echo. The wavelength is reduced. **(C)** If the RBC moves away from this pulse, the frequency of the returning echo is reduced, and its wavelength is increased. This negative Doppler shift is displayed as a blue signal in the standard Color Doppler mode, whereas blood flow moving in the direction of the probe is displayed in red hue.

Doppler Ultrasound

Introduction

Doppler ultrasound provides information on the presence, direction, and speed of blood flow. A detailed description of Doppler ultrasound is beyond the scope of this Atlas, but the reader is encouraged to consult reference textbooks and articles for further understanding of its concepts (Revzin et al. 2019; Szabo and Kaczkowski 2023).

Doppler ultrasound is based on the interaction of ultrasound with particles in movement leading to a change in the frequency of the echoes received, this phenomenon is known as the ***Doppler effect*** (Figure 1.12) (Boote 2003). This effect is displayed and evaluated with color schemes when using color or power Doppler modes or graphically with spectral Doppler (Figures 1.13, 1.14). The numerous applications of these modes are highlighted in several figures throughout this book, and particularly in Chapter 16.

Flow Imaging Modes

With ***Color Doppler***, a color map is used to display the direction and velocity of the blood flow. The size and location of the interrogation box are adjusted to provide an overall view of the flow in a given region, superimposed on the B-mode image for anatomical localization. Color Doppler is essential for cardiac evaluation (see Chapter 6) but can also serve in the assessment of other body parts. It allows rapid identification of vessels and evaluation of their flow characteristics as well as detecting aberrant vessels such as portosystemic shunts or arteriovenous fistulas and assessing tissue perfusion. Color Doppler mode requires that color maps and B-mode data are acquired simultaneously, limiting temporal resolution, and often reducing the spatial resolution of the underlying B-mode image. Limiting the size of the area of color investigation to the region of interest helps to increase the frame rate, thus improving temporal resolution. Color gain should also be carefully adjusted so that the color signals does not extend beyond vascular walls.

Power Doppler Imaging (PDI) – also known as Energy or Angio Doppler – is more sensitive to flows of low velocity as it displays the summation of all the Doppler shift signals rather than the mean in a given area. This mode is favored for confirming the presence of blood flow, particularly in smaller vessels, or to differentiate blood vessels from other tubular structures such as the common bile duct. When combined with directional PDI maps, this mode can also show flow direction (Figure 1.13) (Kennelly and Moran 2008).

Spectral (or Pulsed wave) Doppler examines blood flow at a specific site and provides detailed graphic analysis of the blood flow. The flow characteristics such as velocity, direction, and uniformity can be precisely assessed over time, i.e., throughout the cardiac cycle (Figure 1.14). Flow velocities and indices can be more accurately measured than with color Doppler.

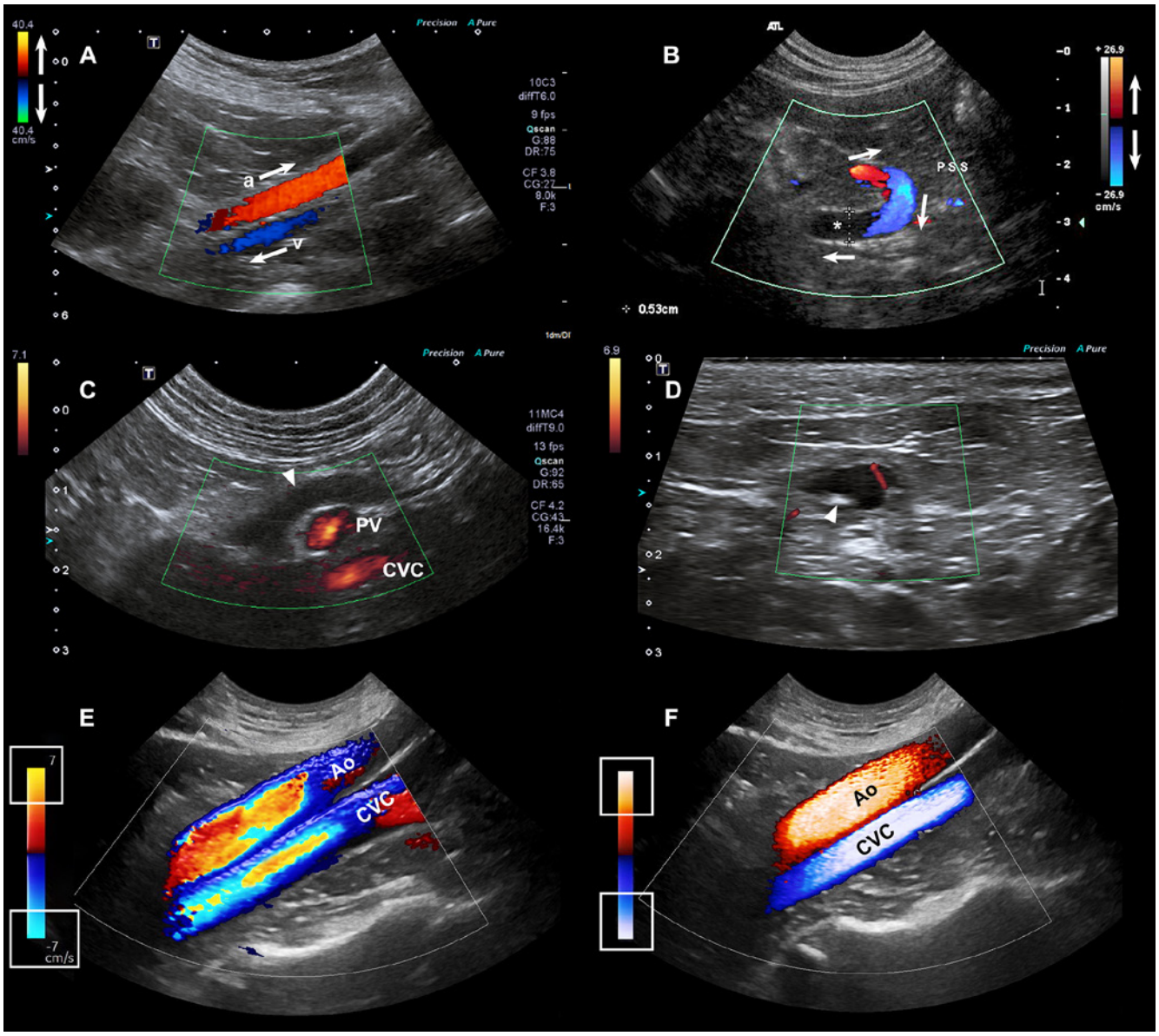

Figure 1.13. **Color and Power Doppler modes. (A)** With color Doppler, the direction of blood flow can be rapidly determined. In this dog, the right external iliac artery (a) and vein (v) show red and blue color hues, indicating flows directed toward and away from the probe, respectively. **(B)** Color hue can change in the same vessel due to a change in direction of the flow, as demonstrated in this tortuous portosystemic shunt (PSS). The arrows indicate the direction of the flow through that shunt. When the flow becomes perpendicular to the probe, a signal void (*) appears because of the lack of Doppler shift. Power Doppler may become useful in such circumstance. **(C)** Power Doppler helps distinguishing this dilated common bile duct (arrowhead) in a cat from the nearby portal vein (PV) and caudal vena cava (CVC). **(D)** Power Doppler may also be used to detect ureteral jet coming from a patent ureter, as opposed to the ipsilateral ureter that is obstructed by a small urolith (arrowhead). **(E, F) Directional Power Doppler imaging**. With conventional color Doppler, the color hues are linked to flow velocity and are affected by scale and pulse repetition frequency (PRF). With the color Doppler settings used in E, flow velocity approaching 7 cm/sec turns from red to yellow when directed toward the transducer and from dark blue to cyan when going away from it (see boxes at the ends of the color scale). When this threshold is exceeded in either direction, flow aliasing occurs, giving a false impression of flow reversal. This is seen in the central part of the aorta (Ao) and CVC that exhibit higher velocities than in the periphery of these vessels. With directional power Doppler, color saturation is rather influenced by the number of moving reflectors; a lighter color indicates more Doppler shift signals perceived, i.e., more moving cells.

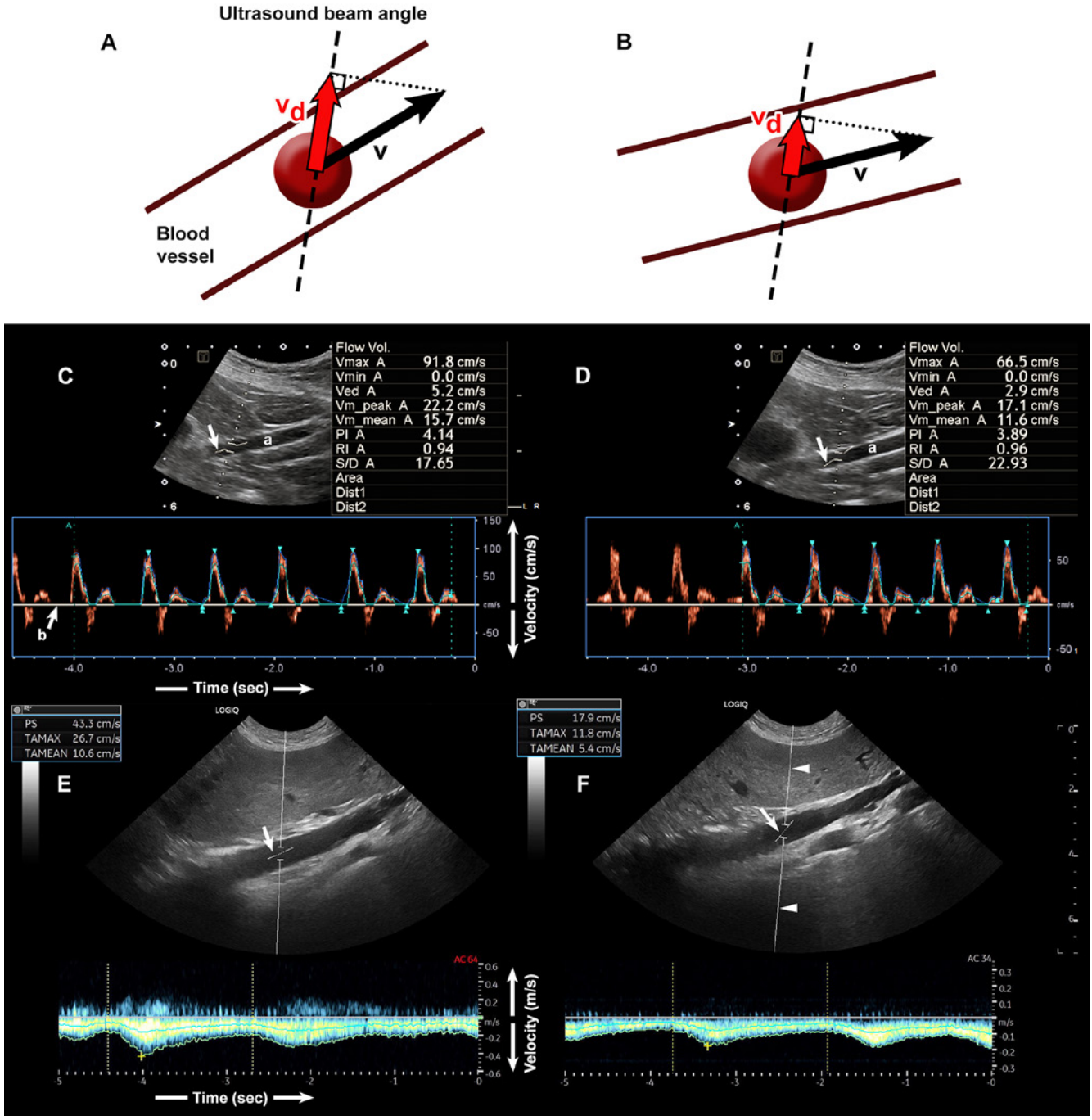

Figure 1.14. Flow velocity measurements using Pulsed (or Spectral) Doppler mode. (A, B) Schematic representation of the impact of flow direction on the estimation of its velocity. Moving blood cells generate a Doppler shift that is used to estimate flow velocity (v_d). When the direction of the flow is more parallel to the axis of the ultrasound beam (such as in A), this Doppler shift is increased, resulting in a higher flow velocity estimation (depicted as the red arrow), whereas, it is lower if the blood flow is more perpendicular (in B). For most accurate estimation of true blood flow velocity (depicted as the black arrows), the angle cursor (in C–F) must be carefully aligned with the direction of the flow. **(C)** The flow in this external iliac artery (a) is mainly directed over the baseline (b), i.e. toward the probe, and pulsates according to the heartbeat. Its changes in direction and velocity are represented over time in this graph. Note that the angle cursor (arrow in B-mode image) was appropriately manually aligned to the long axis of the vessel to measure the velocity vector along that line, which reaches a maximum of 91.8 cm/s and a mean of 15.7 cm/s. **(D)** Changing the angle of this line cursor results in measurement errors. The ultrasound unit estimates the flow velocities based on the measurement of the Doppler shift along that line (66.5 and 11.6 cm/s for maximal and mean velocities, respectively). **(E)** In this dog with hepatitis, the portal venous flow is normally directed toward the liver, smoothly undulating during respiration, with a mean velocity of 10.6 cm/sec. **(F)** Note in this case how flow mean velocity is underestimated (5.4 cm/s) when the angle is not aligned to the long axis of the vein. Manual correction of the velocity vector (arrow) helps the system computer to better estimate true flow velocity along that linear cursor, which must be constantly adjusted since abdominal vessels are examined with variable angles. PS, peak systole velocity; TAMAX, time-averaged maximum velocity; TAMEAN, Time-averaged mean velocity.

In fact, the flow patterns of normal and abnormal abdominal vessels have been well described in dogs (d'Anjou et al. 2004; Szatmari et al. 2001) (see Chapter 16). Sonographers should, however, be careful to measure flow using insonation angles – which can be manually adjusted in the sampling window – well aligned to flow movement and not exceeding 60° to limit measurement errors (Figure 1.14).

Artifacts

Introduction

Artifacts are omnipresent in ultrasound, they are often part of the images and may lead to misinterpretations (Hedrick and Peterson 1995; Kirberger 1995; Feldman et al. 2009; Hindi et al. 2013). In medical ultrasound, it is assumed that (i) ultrasound waves always travel in straight lines from their emitting point; (ii) the lateral width and depth of the beam are narrow and constant; (iii) each interface generates a single reflection; (iv) the intensity and location of echoes displayed as pixels on the monitor truly correspond to the reflecting power and anatomical location of structures being scanned; (v) the speed of the ultrasound waves and the coefficient of attenuation are constant within tissues; and that (vi) each echo seen on the screen comes from the most recently transmitted wave. These assumptions are theoretical, and the sound interaction with biological tissues is complex and responsible for many explained and unexplained artifacts. In addition, the understanding of physical properties of artifacts has been studied *in vitro* by several authors (Barthez et al. 1997; Heng and Widmer 2010), but these conditions are not well representing the complexity of numerous factors such as probe frequency, shape, operator settings, nature, and depth of tissues evaluated.

Deleterious artifacts such as gas-induced reverberation can be partly controlled by adequate patient preparation, scanning methods, and system adjustments. Gastrointestinal content is responsible for most artifacts and can partially be reduced by fasting animals before their exam. Poor contact between the probe and the skin, due to hair, debris, or crusts also limits the transmission and reception of ultrasound waves.

Although artifacts are often responsible for image degradation, they can help interpreting images in many instances (Baad et al. 2017). Their recognition is used to detect and confirm the presence of calculi or tissue mineralization, gas, cysts, and foreign bodies.

Acoustic Shadowing

Shadowing is a zone of echoes with reduced amplitude, beyond a highly attenuating or reflective structure. Most of the incident beam is absorbed and/or reflected at the interface. A uniformly anechoic shadow is called clean, while the term dirty shadowing is used when the shadow is inhomogeneous (Hindi et al. 2013; Rubin et al. 1991).

Clean shadowing is encountered when absorption of the incident beam happens at a hyperattenuating interface such as bone, calculi, or compact foreign material that is larger than the ultrasound beam width (Figure 1.15A-B). The shadow may be partial behind calcifications and calculi that measure less than 0.5mm (Hindi et al. 2013), especially when compound imaging is used. Partial shadowing may also appear behind fat or fibrosis (Hindi et al. 2013; Mesurolle et al. 2002), depending on their size, on the attenuation characteristics of the background tissue and on the equipment and settings.

Dirty shadowing is present when the incident beam is mostly reflected, like at a soft tissue-gas interface (Figure 1.15C–E).

Edge shadowing appears as discrete, triangular zones of low amplitude, at the edge of a curved structure (Figure 1.16A, B). When, the curved structure is fluid filled, the edge shadowing artifact borders the enhancement artifact. This type of refractive shadowing can be confusing, especially when it occurs at the cranial aspect of a fluid filled bladder and appears as a "defect" of the wall (Figure 1.16C–D).

Acoustic Enhancement or Increased Through-transmission

Conversely, waves encountering a structure that allows them to pass through more easily (poorly attenuating), such as a liquid-filled cyst, remain of higher intensity when reaching the deeper tissues, allowing echoes of greater strength to come back to the probe. Consequently, these deeper tissues present an artifactual increase in echogenicity (Figure 1.17). **Acoustic enhancement** is typically recognized deep to a fluid-filled structure in a soft tissue background, such as deep to the gallbladder or to a liver cyst, making them easy to identify and distinguish from solid lesions. Tissues deep to the urinary bladder and organs floating in ascites often become hyperechoic.

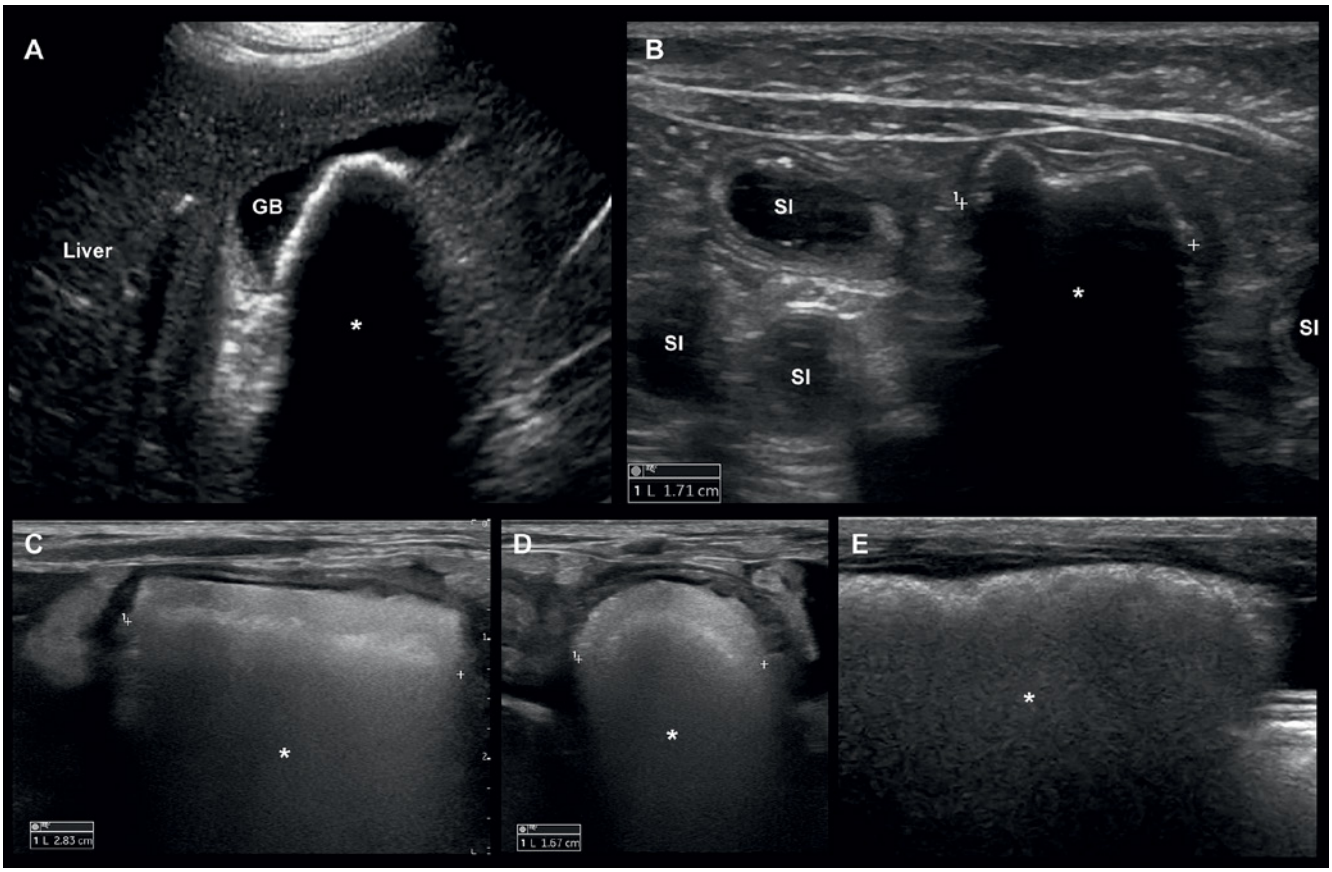

Figure 1.15. **Acoustic shadowing** is a poorly echoic to anechoic zone located below a highly attenuating interface. **(A)** The clean shadow (*) behind this large gallbladder cholelith has the triangular shape of the microconvex probe that was used. **(B)** In this cat, an irregular 1.7-cm-wide foreign body is present in the small intestine, creating a clean shadow (*) that has a more rectangular shape using a linear probe. Nearby small intestinal (SI) loops are filled with fluid. **(C, D)** In this other vomiting cat, there is a cylindrical hyperechoic structure inside the stomach that creates a dirty shadow (*), which was confirmed to represent a foam ear plug. Note the shape of this foreign body in longitudinal **(C)** and transverse **(D)** views as well as the rectangular shape of the artifact using a linear probe. **(E)** Dirty shadowing is also often seen distal to the colon containing gas and stools.

Reverberation

Reverberation artifacts typically appear as a series of multiple equally spaced lines (Figure 1.18A). They occur when the beam hits a highly reflective interface, such as lung, gas in the GI tract or an air pocket, and sends it back as an echo of similar intensity. The high-intensity echo is partly captured by the probe, producing a hyperechoic line at the contact interface, but no echo coming from deeper tissue. The surface of the probe will reflect this high intensity echo and send it back and forth. Since part of the echo is perceived each time it returns, the computer calculates the time passed since the initial launch of the wave pulse and thus records several equidistant hyperechogenic lines. There is decreasing echogenicity of the interface as it goes deeper, due to a gradual loss of wave intensity that rebounds and is attenuated during its trajectory.

Comet tail is a type of reverberation artifact, it appears as a series of short and very closely spaced successive echoes (Figure 1.18B,C,D) that typically decrease in intensity and width in depth. When gas bubbles form thin layers separated by liquid – as in the digestive tract – the waves rebound between the layers, resulting in many echoes that return to the probe at regular intervals, forming a trail of echoes forming a shadow resembling a comet's tail. This artefact is also encountered with metallic pellets and surgical clips (Figure 1.18C). **Ring down artifact** similarly appears as a series of parallel reflective lines that typically extend behind a gas collection. It happens when air bubbles resonate at the ultrasound frequency and then emit reflections. This can be seen associated with gas inside irregular lung surfaces, GI tract, pneumoperitoneum and abscesses. Practically, comet tail and ring down artifacts appear very similar on the screen, even though they result from different physical interactions.